Quantum Information and Computation, Vol. 7, No. 7 (2007) 594–608
© Rinton Press

HIGH-FIDELITY SINGLE-QUBIT GATES USING NON-ADIABATIC RAPID PASSAGE

RAN LI, MELIQUE HOOVER, and FRANK GAITAN
Department of Physics, Southern Illinois University
Carbondale, IL 62901-4401
Department of Physics, Southern Illinois University
Carbondale, IL 62901-4401

Received October 21, 2006
Revised March 16, 2007

Numerical simulation results are presented which suggest that a class of non-adiabatic rapid passage sweeps first realized experimentally in 1991 should be capable of implementing a set of quantum gates that is universal for one-qubit unitary operations and whose elements operate with error probabilities $P_e < 10^{-4}$. The sweeps are non-composite and generate controllable quantum interference effects which allow the one-qubit gates produced to operate non-adiabatically while maintaining high accuracy. The simulations suggest that the one-qubit gates produced by these sweeps show promise as possible elements of a fault-tolerant scheme for quantum computing.

Keywords: quantum computation, quantum interference, resonance, non-adiabatic dynamics
Communicated by: I Cirac & C Williams

1 Introduction

During the years 1997-1998 a number of researchers [1]–[7] showed that under appropriate circumstances a quantum computation of arbitrary duration could be carried out with arbitrarily small error probability in the presence of noise and imperfect quantum logic gates. The conditions that underlie this remarkable result are that: (1) computational data is protected by a sufficiently layered concatenated quantum error correcting code; (2) fault-tolerant protocols for quantum computation are used; and (3) all quantum gates used in the computation have error probabilities[a] P_e that fall below a value known as the accuracy threshold P_a. One of the central challenges facing the field of quantum computing is determining how to implement quantum gates with error probabilities satisfying $P_e < P_a$. The accuracy threshold has been calculated for a number of simple noise models yielding results in the range $10^{-6} < P_a < 10^{-3}$. For many $P_a \sim 10^{-4}$ has become a rough-and-ready working estimate for the threshold so that gates are anticipated to be approaching the accuracies needed for fault-tolerant quantum computing when $P_e < 10^{-4}$. A number of universal sets of quantum gates have been found [8]–[12] and so the problem of producing sufficiently accurate quantum gates has shifted to producing a sufficiently accurate universal set of such gates. One well-known universal set consists of the single-qubit Hadamard, phase, and $\pi/8$ gates together

[a]In this paper all gate error probabilities are per-operation.

with the two-qubit controlled-NOT gate [13]. The single-qubit gates in this set are sufficient to construct any single-qubit unitary operation.

In this paper numerical simulation results are presented which suggest that an existing class of non-adiabatic rapid passage sweeps [14] should be capable of implementing a set of quantum gates $\mathcal{S}_1$ that is universal for one-qubit unitary operations. The one-qubit gates in $\mathcal{S}_1$ are the Hadamard, NOT, V_p, and $V_{\pi/8}$ gates. The universality of $\mathcal{S}_1$ for one-qubit unitary operations is established by noting that the Hadamard gate is an element, and demonstrating that the phase and $\pi/8$ gates can be constructed from the V_p, $V_{\pi/8}$, and NOT gates. This is done in Section 3. For each of the gates in $\mathcal{S}_1$, sweep parameter values are presented which simulations indicate will yield gates that operate non-adiabatically and with error probabilities $P_e < 10^{-4}$. This level of accuracy is a consequence of controllable quantum interference effects that are generated by these sweeps [15]. We explain the optimization procedure used to search for sweep parameter values that (when successful) yield this high degree of gate accuracy.

The outline of this paper is as follows. In the following Section we summarize the necessary background associated with this class of non-adiabatic rapid passage sweeps; Section 3 presents our simulation results for the different gates; and Section 4 discusses these results, their relation to existing work in the literature, and also current challenges.

2 Twisted Rapid Passage

We consider a qubit that couples to an external control field $\mathbf{F}(t)$ through the Zeeman interaction:

$$H(t) = \boldsymbol{\sigma} \cdot \mathbf{F}(t) \quad , \tag{1}$$

where $\boldsymbol{\sigma}$ are the Pauli matrices. The sweeps we will be interested in are a generalization of those used in adiabatic rapid passage (ARP). In ARP the field $\mathbf{F}(t)$ in the detector frame [16] is inverted over a time T_0 such that $\mathbf{F}(t) = b\,\hat{\mathbf{x}} + at\,\hat{\mathbf{z}}$. In an NMR realization of ARP, as seen in the lab frame, the detector frame rotates about the static magnetic field $B_0\,\hat{\mathbf{z}}$. In the detector frame, $\hat{\mathbf{z}}$ is chosen to be parallel to the rotation axis. In the rotating wave approximation the rf-magnetic field $\mathbf{B}_{rf}$ in the lab frame lies in the x-y plane and rotates about the static magnetic field. The detector frame is chosen to rotate with $\mathbf{B}_{rf}$ so that in this frame the rf field is static and its direction defines $\hat{\mathbf{x}}$: $\mathbf{B}_{rf} = b\hat{\mathbf{x}}$. The inversion time T_0 is large compared to the inverse Larmor frequency ω_0^{-1} (viz. adiabatic), though small compared to the thermal relaxation time τ_{th} (viz. rapid). It provides a highly precise method for inverting the qubit Bloch vector $\mathbf{s} = \langle\boldsymbol{\sigma}\rangle$, although the price paid for this precision is an adiabatic inversion rate. We are interested in a type of rapid passage in which the control field $\mathbf{F}(t)$ as seen in the detector frame is allowed to twist around in the x–y plane with azimuthal angle $\phi(t)$ while simultaneously undergoing inversion along the z-axis:

$$\mathbf{F}(t) = b\cos\phi(t)\,\hat{\mathbf{x}} + b\sin\phi(t)\,\hat{\mathbf{y}} + at\,\hat{\mathbf{z}} \quad . \tag{2}$$

Here $-T_0/2 \leq t \leq T_0/2$ and $\hat{\mathbf{y}} = \hat{\mathbf{z}} \times \hat{\mathbf{x}}$. Note that any pair of orthogonal unit vectors in the x–y plane can be used for $\hat{\mathbf{x}}$ and $\hat{\mathbf{y}}$. Different choices simply alter the value of $\phi(t = 0)$. As will be explained shortly, interesting physical effects arise when the twist profile $\phi(t)$ is chosen appropriately. This type of rapid passage is referred to as twisted rapid passage (TRP). The first experimental realization of TRP in 1991 by Zwanziger et. al. [14] carried out the inversion adiabatically with $\phi(t) = Bt^2$. Since then, non-adiabatic TRP has been studied with polynomial twist profile $\phi(t) = (2/n)Bt^n$ [15], and controllable quantum interference effects were found to arise for $n \geq 3$. Zwanziger et. al. [17] implemented non-adiabatic polynomial TRP with $n = 3, 4$ and observed the predicted interference effects. In the following subsection we briefly summarize how these quantum interferences arise and refer the reader to Ref. [15] for further discussion.

2.1 Controllable Quantum Interference

In the Zwanziger experiments [14, 17], a TRP sweep is produced by sweeping the detector frequency linearly through resonance at the Larmor frequency ω_0: $\dot{\phi}_{det}(t) = \omega_0 + (2at)/\hbar$. The frequency of the rf-field $\dot{\phi}_{rf}$ is also swept through resonance in such a way that $\dot{\phi}_{rf}(t) = \dot{\phi}_{det}(t) - \dot{\phi}(t)$, where $\phi(t) = (2/n)Bt^n$ is the TRP twist profile. Thus,

$$\begin{aligned} \dot{\phi}_{rf}(t) &= \dot{\phi}_{det}(t) - \dot{\phi}(t) \\ &= \omega_0 + \frac{2at}{\hbar} + \dot{\phi}(t) \quad . \end{aligned} \tag{3}$$

At resonance $\dot{\phi}_{rf}(t) = \omega_0$. Inserting this condition into eq. (3), it follows that at resonance:

$$at - \frac{\hbar}{2}\frac{d\phi}{dt} = 0 \quad . \tag{4}$$

As shown in Ref. [15], for polynomial twist $\phi(t) = (2/n)Bt^n$ with $n \geq 3$, eq. (4) has $n - 1$ roots, though only the real-valued roots correspond to resonance. The various possibilities are summarized in Table 1. We see that: (i) for $B > 0$ a qubit always passes through resonance

Table 1. Classification of regimes under which multiple qubit resonances occur for polynomial twist $\phi(t) = (2/n)Bt^n$ with $n \geq 3$.

	1. $\underline{B > 0}$	
(a) n odd:	2 resonances at	$t = 0$ and $t = (a/\hbar B)^{\frac{1}{n-2}}$
(b) n even:	3 resonances at	$t = 0$ and $t = \pm\,(a/\hbar B)^{\frac{1}{n-2}}$
	2. $\underline{B < 0}$	
(a) n odd:	2 resonances at	$t = 0$ and $t = -\,(a/\hbar \lvert B\rvert)^{\frac{1}{n-2}}$
(b) n even:	1 resonance at	$t = 0$

multiple times during a *single* TRP sweep; (ii) for $B < 0$ multiple resonances only occur when n is odd; and (iii) the time separating qubit resonances can be altered by variation of the sweep parameters B and a. Ref. [15] showed that these multiple resonances have a strong influence on the qubit transition probability. It was shown that qubit transitions could be significantly enhanced or suppressed by small variation of the sweep parameters, and hence of the time separating the resonances. Plots of the transition probability versus time suggested that the multiple resonances were producing quantum interference effects that could be controlled by variation of the TRP sweep parameters. In Ref. [18] the qubit transition amplitude was calculated to all orders in the non-adiabatic coupling. The result found there can be re-expressed as the following diagrammatic series:

$T_{-}(t) =$ 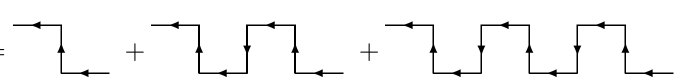 $+ \cdots \quad .$ (5)

Lower (upper) lines correspond to propagation in the negative (positive) energy level and the vertical lines correspond to transitions between the two energy levels. The calculation sums the probability amplitudes for all interfering alternatives [19] that allow the qubit to end up in the positive energy level at time t given that it was initially in the negative energy level. As we have seen, varying the TRP sweep parameters varies the time separating the resonances. This in turn changes the value of each diagram in eq. (5), and thus alters the interference between alternatives in this quantum superposition. Similar diagrammatic series can be worked out for the remaining 3 combinations of final and intial states. It is the sensitivity of the individual alternatives/diagrams to the time separation of the resonances that allows TRP to manipulate this quantum interference. Zwanziger et. al. [17] observed these interference effects in the transition probability using liquid state NMR and found quantitative agreement between theory and experiment. It is the link between the TRP sweep parameters and this quantum interference that we believe makes it possible for TRP to drive highly accurate single-qubit gates that operate non-adiabatically. The results presented in Section 3 for the different single-qubit gates are found by numerical simulation of the one-qubit Schrodinger equation. We next briefly describe how these simulations are done [15].

2.2 Simulation Protocol

As is well-known, the Schrodinger dynamics implements a unitary transformation $U(t, t_0)$ of the initial quantum state $|\psi(t_0)\rangle$:

$$|\psi(t)\rangle = U(t, t_0)\, |\psi(t_0)\rangle \quad . \tag{6}$$

An n-qubit quantum gate implements a fixed unitary transformation U on n qubits. The unitary transformations U_H, U_P, $U_{\pi/8}$, and U_{NOT} carried out by the one-qubit Hadamard, phase, $\pi/8$, and NOT gates are, respectively,

$$U_H = \frac{1}{\sqrt{2}} \begin{pmatrix} 1 & 1 \\ 1 & -1 \end{pmatrix} \qquad U_P = \begin{pmatrix} 1 & 0 \\ 0 & i \end{pmatrix} \tag{7}$$

$$U_{\pi/8} = \begin{pmatrix} 1 & 0 \\ 0 & e^{i\pi/4} \end{pmatrix} \qquad U_{NOT} = \begin{pmatrix} 0 & 1 \\ 1 & 0 \end{pmatrix} \quad . \tag{8}$$

All matrices are in the representation spanned by the computational basis states $|0\rangle$ and $|1\rangle$ which are chosen to be eigenstates of σ_z:

$$\sigma_z\, |i\rangle = (-1)^i\, |i\rangle \qquad (i = 0, 1) \quad .$$

To determine the dynamical impact of TRP, the 1-qubit Schrodinger equation is simulated numerically in the non-rotating frame in which the Hamiltonian $H(t)$ is given by eqs. (1) and (2). It is found that the numerical stability of the simulation is enhanced if we expand the state $|\psi(t)\rangle$ in the instantaneous energy eigenstates $|E_{\pm}(t)\rangle$ for which $H(t)|E_{\pm}(t)\rangle = E_{\pm}(t)|E_{\pm}(t)\rangle$. Because of the direct connection between these states and $H(t)$, they carry substantial dynamical information, and a substantial portion of the dynamics due to $H(t)$ can be accounted for by choosing this basis. This makes the task of determining the remaining dynamics using the Schrodinger equation much simpler and the simulation more stable. We thus write:

$$|\psi(t)\rangle = S(t) \exp\left[-\frac{i}{\hbar}\int_{-T_0/2}^{t} d\theta\,(E_- - \hbar\dot{\gamma}_-)\right]|E_-(t)\rangle$$
$$-I(t)\exp\left[-\frac{i}{\hbar}\int_{-T_0/2}^{t} d\theta\,(E_+ - \hbar\dot{\gamma}_+)\right]|E_+(t)\rangle\ . \qquad (9)$$

Here $\gamma_{\pm}(t)$ are the adiabatic geometric phases [20] associated with the energy levels $E_{\pm}(t)$, respectively, and

$$\dot{\gamma}_{\pm}(t) = i\langle E_{\pm}(t)|\frac{d}{dt}|E_{\pm}(t)\rangle \quad .$$

Substituting eq. (9) into the Schrodinger equation leads to the equations of motion for $S(t)$ and $I(t)$:

$$\begin{aligned} \frac{dS}{dt} &= -\Gamma^*(t)\,\exp\left[-i\int_{-T_0/2}^{t} d\theta\,\delta(\theta)\right]\,I(t) \\ \frac{dI}{dt} &= \Gamma(t)\,\exp\left[i\int_{-T_0/2}^{t} d\theta\,\delta(\theta)\right]\,S(t)\quad , \end{aligned} \qquad (10)$$

where

$$\begin{aligned} \delta(t) &= \frac{E_+(t) - E_-(t)}{\hbar} - [\,\dot{\gamma}_+(t) - \dot{\gamma}_-(t)\,] \\ \Gamma(t) &= \langle E_+(t)|\frac{d}{dt}|E_-(t)\rangle \quad , \end{aligned}$$

and $\Gamma^*(t) = -\langle E_-(t)|d/dt|E_+(t)\rangle$. The qubit is initially placed in one of the initial instantaneous energy eigenstates $|\psi(-T_0/2)\rangle = |E_{\pm}(-T_0/2)\rangle$ which fixes the initial condition for $S(t)$ and $I(t)$ through eq. (9). It proves useful to recast eqs. (10) in dimensionless form. To that end one introduces the dimensionless time $\tau = (a/b)t$, the dimensionless inversion rate $\lambda = \hbar|a|/b^2$, and the dimensionless twist strength $\eta_n = (\hbar B/a)(b/a)^{n-2}$. The connection between these dimensionless simulation parameters and the experimental sweep parameters is given in Section 3. It is straightforward to show that the resonances in Table 1 occur at [15]:

$$\tau = 0 \quad , \qquad (11)$$

and

$$\tau = (\mathrm{sgn}\,\eta_n)^{\frac{1}{(n-2)}}\left[\frac{1}{|\eta_n|}\right]^{\frac{1}{(n-2)}} \quad , \qquad (12)$$

though only the real-valued solutions of eqs. (11) and (12) correspond to qubit resonances. The dimensionless version of eqs. (10) are the equations that are numerically integrated. The simulations allow us to determine the actual unitary transformation U_a produced by a specific assignment of the TRP sweep parameters T_0, a, b, B, and n. Section 2.4 will explain how the sweep parameters are iteratively modified so as to make U_a approach a target gate U_t as closely as possible. The iterative procedure searches for a sweep parameter set which minimizes (an upper bound for) the error probability P_e for U_a relative to U_t. We next explain how P_e and its upper bound are determined.

2.3 Gate Error Probability

The following argument is for an N-dimensional Hilbert space, though $N = 2$ will be the case of interest in this paper. As in Section 2.2, let U_a denote the actual unitary operation produced by a given set of TRP sweep parameters and U_t a target unitary operation we would like TRP to approximate as closely as possible. Introducing the operators $D = U_a - U_t$ and $P = D^\dagger D$, and the normalized state $|\psi\rangle$, we define $|\psi_a\rangle = U_a|\psi\rangle$ and $|\psi_t\rangle = U_t|\psi\rangle$. Now choose an orthonormal basis $|i\rangle$ $(i = 1, \ldots, N)$ such that $|1\rangle \equiv |\psi_t\rangle$ and define the state $|\xi_\psi\rangle$ via

$$\begin{aligned} |\psi_a\rangle &= |\psi_t\rangle + |\xi_\psi\rangle && (13) \\ &= |1\rangle + |\xi_\psi\rangle \quad . && (14) \end{aligned}$$

Inserting $|\xi_\psi\rangle = \sum_{i=1}^{N} e_i|i\rangle$ into eq. (14) gives

$$|\psi_a\rangle = (1 + e_1)\,|1\rangle + \sum_{i\neq 1} e_i|i\rangle \quad . \tag{15}$$

Since $|\psi_t\rangle = |1\rangle$ is the target state, it is clear from eq. (15) that the error probability $P_e(\psi)$ for U_a (i. e. TRP) is

$$P_e(\psi) = \sum_{i\neq 1} |e_i|^2 \quad . \tag{16}$$

We define the error probability P_e for the TRP gate to be

$$P_e \equiv \max_{|\psi\rangle} P_e(\psi) \quad . \tag{17}$$

From eq. (13),

$$|\xi_\psi\rangle = D|\psi\rangle$$

and

$$\begin{aligned} \langle\xi_\psi|\xi_\psi\rangle &= \langle\psi|D^\dagger D|\psi\rangle \\ &= Tr\rho_\psi P \quad , && (18) \end{aligned}$$

where $\rho_\psi = |\psi\rangle\langle\psi|$. On the other hand,

$$\begin{aligned} \langle\xi_\psi|\xi_\psi\rangle &= \sum_{i=1}^{N} |e_i|^2 \\ &= |e_1|^2 + P_e(\psi) \quad . && (19) \end{aligned}$$

Combining eqs. (18) and (19) gives

$$\begin{aligned} P_e(\psi) &= \langle\xi_\psi|\xi_\psi\rangle - |e_1|^2 \\ &\leq \langle\xi_\psi|\xi_\psi\rangle = Tr\rho_\psi P \quad . \end{aligned}$$

Since $P = D^\dagger D$ is Hermitian it can be diagonalized: $P = O^\dagger d\,O$ and $d = diag(d_1, \ldots, d_N)$. Thus

$$P_e(\psi) \leq Tr\,\overline{\rho}_\psi d \quad ,$$

where $\overline{\rho}_\psi = O\rho_\psi O^\dagger$. Let $d_* = \max(d_1, \ldots, d_N)$, then direct evaluation of the trace gives

$$
\begin{aligned}
Tr\,\overline{\rho}_\psi d &= \sum_{i=1}^{N} d_i \left(\overline{\rho}_\psi\right)_{ii} \\
&\leq \sum_{i=1}^{N} d_* \left(\overline{\rho}_\psi\right)_{ii} = d_*\, Tr\,\overline{\rho}_\psi = d_* \quad ,
\end{aligned}
$$

where we have used that $Tr\,\overline{\rho}_\psi = 1$. Thus $P_e(\psi) \leq d_*$ for *all* states $|\psi\rangle$. From eq. (17), it follows that

$$P_e \leq d_* \quad , \tag{20}$$

so that the largest eigenvalue d_* of P is an upper bound for the gate error probability P_e. Finally, notice that $P = D^\dagger D$ is a positive operator so that $d_i \geq 0$ for $i = 1, \ldots, N$. Thus $d_* \leq Tr\,P$ and so

$$P_e \leq d_* \leq Tr\,P \quad . \tag{21}$$

Although $Tr\,P$ need not be as tight an upper bound on P_e as d_*, it is much easier to calculate and so is more convenient than d_* for use in the sweep optimization procedure to be described next.

2.4 Sweep Optimization Procedure

To find TRP sweep parameters that yield highly accurate non-adiabatic one-qubit gates we used the multi-dimensional downhill simplex method [21] to search for sweep parameters that minimize the upper bound $Tr\,P$ for the gate error probability P_e. Although we simulated a number of different types of polynomial twist, all data presented in Section 3 will be for quartic twist, $\phi_4(\tau) = (\eta_4/2\lambda)\,\tau^4$, which yielded the best results. The sweep parameters for quartic twist are (λ, η_4) which can be thought of as specifying a point in a 2-dimensional parameter space. For quartic twist, the downhill simplex method takes as input 3 sets of sweep parameters which specify the vertices of a simplex in the 2-dimensional parameter space. The dynamical effects of the TRP sweep associated with each vertex is found by numerically integrating the one-qubit Schrodinger equation as described in Section 2.2. The output of the integration is the unitary operation U_a that a particular sweep applies. The desire is to iteratively improve U_a so that it approximates as closely as possible a target unitary operation U_t. For each U_a we determine $P = (U_a - U_t)^\dagger (U_a - U_t)$ and evaluate $Tr\,P$. The downhill simplex method then iteratively alters the simplex (i. e. one or more of its vertices) until sweep parameters are found that yield a local minimum of $Tr\,P$. Because this minimum is not global, some starting simplexes will give deeper minimums than others. Though there was no gaurantee, it was hoped that a starting simplex could be found that yielded $Tr\,P < 10^{-4}$. Some trial and error in specifying the starting simplex was thus required, though for one-qubit gates, the trial and error procedure eventually proved successful and we present our results in the following Section.

3 Simulation Results

All results presented below are for quartic twist

$$\phi(\tau) = \frac{1}{2}\left(\frac{\eta_4}{\lambda}\right)\tau^4 \quad , \tag{22}$$

where τ, λ, and η_4 are the dimensionless versions of time t, inversion rate a, and twist strength B (Section 2.2). For convenience, we re-write their definitions here:

$$\tau = \left(\frac{a}{b}\right) t \quad ; \quad \lambda = \frac{\hbar|a|}{b^2} \quad ; \quad \eta_4 = \left(\frac{\hbar b^2}{a^3}\right) B \quad . \tag{23}$$

The parameter b was introduced in eq. (2) and is the rf field amplitude in an NMR realization of TRP [17, 15]. All simulations were done with $\lambda > 1$ corresponding to non-adiabatic inversion [17, 15], and with $\tau_0 = aT_0/b = 80.000$.

The translation key connecting our dimensionless simulation parameters and the experimental sweep parameters used in the Zwanziger experiments [14, 17] was given in the Appendix of Ref. [15]. We re-write the formulas for quartic twist here for convenience. Note that Zwanziger's symbol B is here replaced by $\mathcal{B}$ to avoid confusion with our use of the symbol B in this paper to denote the twist strength. The translation formulas are:

$$\omega_1 = \frac{2b}{\hbar} \tag{24}$$

$$A = \frac{aT_0}{\hbar} \tag{25}$$

$$\mathcal{B} = \frac{BT_0^4}{2} \tag{26}$$

$$\lambda = \frac{4A}{\omega_1^2 T_0} \tag{27}$$

$$\eta_4 = \frac{\mathcal{B}\omega_1^2}{2A^3 T_0} \quad . \tag{28}$$

In the experiments of Ref. [17]: $\omega_1 = 393Hz$; $T_0 = 41.00ms$; $A = 50\,000Hz$; and $\mathcal{B}$ was calculated from eq. (28) with η_4 varying over the range $[4.50, 4.70] \times 10^{-4}$.

Note that U_P and $U_{\pi/8}$ (see eqs. (7) and (8)) can be re-written as

$$U_P = e^{i\pi/4}\, U_{NOT}\, V_P \tag{29}$$

$$U_{\pi/8} = e^{i\pi/8}\, U_{NOT}\, V_{\pi/8} \quad , \tag{30}$$

where

$$V_P = \begin{pmatrix} 0 & e^{i\pi/4} \\ e^{-i\pi/4} & 0 \end{pmatrix} \tag{31}$$

$$V_{\pi/8} = \begin{pmatrix} 0 & e^{i\pi/8} \\ e^{-i\pi/8} & 0 \end{pmatrix} \quad , \tag{32}$$

and U_{NOT} is given in eq. (8). As will be seen below, our simulations produced V_P and $V_{\pi/8}$, from which U_P and $U_{\pi/8}$ can be constructed using eqs. (29) and (30), respectively. TRP is thus used to construct the set of gates $\mathcal{S}_1 = \{U_H, V_P, V_{\pi/8}, U_{NOT}\}$ which is universal for one-qubit unitary gates. We stress that all gates in this set are produced using a non-composite TRP sweep (eq. (2)). The different gates result from different choices for the TRP sweep parameters. For each one-qubit gate, we present our best-case results and show how gate performance is altered by small variations in the sweep parameters.

Hadamard Gate

The sweep parameters $\lambda = 5.8511$ and $\eta_4 = 2.9280 \times 10^{-4}$ produce the gate U_a whose real and imaginary parts are:

$$Re(U_a) = \begin{pmatrix} 0.708581 & 0.705629 \\ 0.705629 & -0.708581 \end{pmatrix} \quad (33)$$

$$Im(U_a) = \begin{pmatrix} 0.380321 \times 10^{-9} & -0.144317 \times 10^{-4} \\ 0.144317 \times 10^{-4} & 0.420313 \times 10^{-9} \end{pmatrix} . \quad (34)$$

For comparison, the real and imaginary parts of the target Hadamard gate $U_t = U_H$ are:

$$Re(U_H) = \begin{pmatrix} 0.707107 & 0.707107 \\ 0.707107 & -0.707107 \end{pmatrix} \quad (35)$$

$$Im(U_H) = \begin{pmatrix} 0 & 0 \\ 0 & 0 \end{pmatrix} . \quad (36)$$

From U_a and U_H we find $Tr\, P = 8.82 \times 10^{-6}$ and so the gate error probability satisfies $P_e \leq 8.82 \times 10^{-6}$. Table 2 shows how gate performance varies when the sweep parameters are altered slightly. Of the two sweep parameters, η_4 variation is seen to have the largest impact on gate performance. This will turn out to be true for the other one-qubit gates as well. Although TRP can produce a Hadamard gate whose error probability falls below the accuracy threshold $P_a \sim 10^{-4}$, it is clear from Table 2 that the sweep parameters must be controlled to 5 significant figures to achieve this level of performance. See Section 4 for further discussion this point.

Table 2. Variation of $Tr\, P$ for the Hadamard gate when the TRP sweep parameters are altered slightly from their best performance values. The columns to the left of center have $\eta_4 = 2.9280 \times 10^{-4}$ and those to the right have $\lambda = 5.8511$.

η_4	λ	$Tr\, P$	λ	η_4	$Tr\, P$
2.9280×10^{-4}	5.8510	7.22×10^{-5}	5.8511	2.9279×10^{-4}	7.03×10^{-4}
	5.8511	8.82×10^{-6}		2.9280×10^{-4}	8.82×10^{-6}
	5.8512	1.84×10^{-5}		2.9281×10^{-4}	6.14×10^{-4}

V_P Gate

As noted above, the target gate here is V_P, and U_P follows from eq. (29). The sweep parameters $\lambda = 5.9750$ and $\eta_4 = 3.8060 \times 10^{-4}$ produce the gate U_a:

$$Re(U_a) = \begin{pmatrix} -0.627432 \times 10^{-2} & 0.706181 \\ 0.706181 & 0.627432 \times 10^{-2} \end{pmatrix} \quad (37)$$

$$Im(U_a) = \begin{pmatrix} -0.284521 \times 10^{-10} & 0.708004 \\ -0.708004 & 0.694222 \times 10^{-11} \end{pmatrix} . \quad (38)$$

From eq. (31), the target gate V_P is:

$$Re(V_P) = \begin{pmatrix} 0 & 0.707107 \\ 0.707107 & 0 \end{pmatrix} \quad (39)$$

$$Im(V_P) = \begin{pmatrix} 0 & 0.707107 \\ -0.707107 & 0 \end{pmatrix} . \quad (40)$$

From U_a and V_P we find $Tr\,P = 8.20 \times 10^{-5}$ and so $P_e \leq 8.20 \times 10^{-5}$ for this gate. Table 3 shows how $Tr\,P$ varies when η_4 and λ are varied slightly. Again gate performance is most sensitive to variation of η_4, and the sweep parameters must be controlled to 5 significant figures for performance to surpass the accuracy threshold. The latter point is discussed further in Section 4.

Table 3. Variation of $Tr\,P$ for the V_P gate when the TRP sweep parameters are altered slightly from their best performance values. The columns to the left of center have $\eta_4 = 3.8060 \times 10^{-4}$ and those to the right have $\lambda = 5.9750$.

η_4	λ	$Tr\,P$	λ	η_4	$Tr\,P$
3.8060×10^{-4}	5.9749	1.56×10^{-4}	5.9750	3.8059×10^{-4}	2.29×10^{-3}
	5.9750	8.20×10^{-5}		3.8060×10^{-4}	8.20×10^{-5}
	5.9751	1.43×10^{-4}		3.8061×10^{-4}	1.88×10^{-3}

$V_{\pi/8}$ **Gate**

From eq. (30), $U_{\pi/8}$ is found from $V_{\pi/8}$ and U_{NOT}. The target gate this time is $V_{\pi/8}$. For $\lambda = 6.0150$ and $\eta_4 = 8.1464 \times 10^{-4}$ TRP produced the gate U_a:

$$Re(U_a) = \begin{pmatrix} 0.101927 \times 10^{-2} & 0.925307 \\ 0.925307 & -0.101927 \times 10^{-2} \end{pmatrix} \quad (41)$$

$$Im(U_a) = \begin{pmatrix} -0.960223 \times 10^{-10} & 0.379218 \\ -0.379218 & 0.184961 \times 10^{-10} \end{pmatrix} . \quad (42)$$

From eq. (32), the target gate $V_{\pi/8}$ is:

$$Re(V_{\pi/8}) = \begin{pmatrix} 0 & 0.923880 \\ 0.923880 & 0 \end{pmatrix} \quad (43)$$

$$Im(V_{\pi/8}) = \begin{pmatrix} 0 & 0.382683 \\ -0.382683 & 0 \end{pmatrix} . \quad (44)$$

These matrices give $Tr\,P = 3.03 \times 10^{-5}$ and so for this gate $P_e \leq 3.03 \times 10^{-5}$. Table 4 shows how gate performance varies when the sweep parameters are altered slightly. As with the previous two gates, performance is most sensitive to variation of η_4, and the sweep parameters must be controllable to 5 significant figures (see Section 4).

Table 4. Variation of $Tr\,P$ for the $V_{\pi/8}$ gate when the TRP sweep parameters are altered slightly from their best performance values. The columns to the left of center have $\eta_4 = 8.1464 \times 10^{-4}$ and those to the right have $\lambda = 6.0150$.

η_4	λ	$Tr\,P$	λ	η_4	$Tr\,P$
8.1464×10^{-4}	6.0149	1.30×10^{-3}	6.0150	8.1463×10^{-4}	1.77×10^{-3}
	6.0150	3.03×10^{-5}		8.1464×10^{-4}	3.03×10^{-5}
	6.0151	2.18×10^{-3}		8.1465×10^{-4}	2.77×10^{-3}

NOT Gate

Finally, we examine U_{NOT}. For $\lambda = 7.3205$ and $\eta_4 = 2.9277 \times 10^{-4}$ TRP produced the gate U_a:

$$Re(U_a) = \begin{pmatrix} 0.235039 \times 10^{-2} & 0.999997 \\ 0.999997 & -0.235039 \times 10^{-2} \end{pmatrix} \quad (45)$$

$$Im(U_a) = \begin{pmatrix} -0.323648 \times 10^{-10} & -0.115151 \times 10^{-4} \\ 0.115150 \times 10^{-4} & 0.271006 \times 10^{-10} \end{pmatrix}. \quad (46)$$

For comparison, U_{NOT} is (eq. (8)):

$$Re(U_{NOT}) = \begin{pmatrix} 0 & 1 \\ 1 & 0 \end{pmatrix} \quad (47)$$

$$Im(U_{NOT}) = \begin{pmatrix} 0 & 0 \\ 0 & 0 \end{pmatrix}. \quad (48)$$

These matrices yield $Tr\,P = 1.10 \times 10^{-5}$ and so $P_e \leq 1.10 \times 10^{-5}$. Table 5 shows how $Tr\,P$ varies with small variation of the sweep parameters. As with the other gates, performance is most sensitive to variation in η_4, and sweep parameters must be controllable to 5 significant figures for the gate error probability P_e to fall below the accuracy threshold $P_a \sim 10^{-4}$ (see Section 4).

Table 5. Variation of $Tr\,P$ for the NOT gate when the TRP sweep parameters are altered slightly from their best performance values. The columns to the left of center have $\eta_4 = 2.9277 \times 10^{-4}$ and those to the right have $\lambda = 7.3205$.

η_4	λ	$Tr\,P$	λ	η_4	$Tr\,P$
2.9277×10^{-4}	7.3204	1.12×10^{-5}	7.3205	2.9276×10^{-4}	1.23×10^{-3}
	7.3205	1.10×10^{-5}		2.9277×10^{-4}	1.10×10^{-5}
	7.3206	1.22×10^{-5}		2.9278×10^{-4}	1.23×10^{-3}

4 Discussion

In this paper we have presented numerical simulation results which suggest that TRP sweeps should be capable of producing a set of quantum gates that is universal for one-qubit unitary operations. We also showed that sweep parameters can be found which the simulations indicate will yield gates that operate non-adiabatically and with error probabilities satisfying $P_e \leq 10^{-4}$. To achieve this degree of accuracy, however, the sweep parameters must be controllable to high precision (5 significant figures). This raises the question of whether such precision is possible with current technology. In the NMR realization of TRP [14, 17] the inversion time T_0 was of order $10^{-2}\,s$, while the spectrometer waveform resolution allowed the rf- and detector-phases to be specified in time steps of order $10^{-7}\,s$. Thus T_0 can be determined to 1 part in 10^5. By using shimming and sample rotation the uncertainty in the Larmor frequency ω_0 (which is used in eqs. (53) and (54)) can be reduced to $15\,Hz$, while its value is $500MHz$. This corresponds to a relative error of $\Delta\omega_0/\omega_0 \sim 10^{-7}$. It is also possible to use π or $\pi/2$ pulses to calibrate the rf field strength ω_1 down to a relative error of $\Delta\omega_1/\omega_1 \sim 10^{-4}$. Thus many of the TRP sweep parameters are already at or near the level of precision needed to make high-fidelity one-qubit gates. Still, it is clear that further theoretical work is needed to find ways to make the gate error probability a more slowly varying function of the TRP sweep parameters. Recall that TRP sweeps are non-composite. It is an interesting open question whether composite sweeps that interlay TRP with different types of pulses can lead to more robust gate performance. We intend to examine this question in our next set of simulations. Having discussed current challenges, it is worth stressing that these sweeps show genuine potential for producing high-fidelity non-adiabatic one-qubit gates. Further work to try to develop this potential seems warranted. Although other approaches exist for making one-qubit gates (e. g. Ref. [23]), in a field faced with as many technical challenges as quantum computing, it is advantageous to have multiple ways to accomplish important tasks. It is hoped that with further development TRP gates may provide an approach to making high-fidelity non-adiabatic quantum gates. TRP sweeps also provide a concrete example of how quantum effects can be used to enhance our control of a quantum system. Further study of these sweeps also seems worthwhile as a question of basic physics.

Atomic Physics

The following scenario is inspired by the NMR realization of TRP [14, 17]. Consider electric dipole transitions between a pair of atomic energy eigenstates $|+\rangle$ and $|-\rangle$ of the Hamiltonian H_a with respective energies $E_\pm = \pm\epsilon_0/2$. Transition between these two states is caused by an applied electric field $\mathbf{E}_a(t) = 2E_1 \cos\phi_a(t)\,\mathbf{x}$ which couples to the atom's electric dipole moment $\mathbf{d} = e\,\mathbf{r}$. In the lab frame, the two-level Hamiltonian $\mathcal{H}(t)$ in the rotating wave approximation is [22]:

$$\mathcal{H}(t) = -\frac{\hbar\omega_0}{2}\,\sigma_z + \frac{\hbar\omega_1}{2}\left[\cos\phi_a(t)\,\sigma_x + \sin\phi_a(t)\,\sigma_y\right] \quad ,$$

where $\hbar\omega_0 = \epsilon_0$ and $\hbar\omega_1 = d_x E_1$. Transformation to the detector frame [14, 16] is done using the unitary operator $U(t) = \exp[-(i/2)\phi_{det}(t)\sigma_z]$ so that $\mathcal{H} \rightarrow \overline{\mathcal{H}}$:

$$\begin{aligned} \overline{\mathcal{H}}(t) &= \frac{\hbar}{2}\left(\dot{\phi}_{det} - \omega_0\right)\sigma_z + \frac{\hbar\omega_1}{2}\left[\cos(\phi_a - \phi_{det})\sigma_x + \sin(\phi_a - \phi_{det})\sigma_y\right] \\ &= at\sigma_z + b\cos\phi_n(t)\sigma_x + b\sin\phi_n(t)\sigma_y \quad , \end{aligned} \tag{49}$$

where

$$at = \frac{\hbar}{2}\left(\dot{\phi}_{det} - \omega_0\right) \tag{50}$$

$$b = \frac{\hbar\omega_1}{2} \tag{51}$$

$$\phi_n(t) = \phi_a - \phi_{det} \quad , \tag{52}$$

and $\phi_n(t) = (2/n)Bt^n$ is the twist profile for polynomial twist. Eq. (49) gives $\overline{\mathcal{H}}(t) = \boldsymbol{\sigma}\cdot\mathbf{F}(t)$, where $\mathbf{F}(t)$ is the control field for TRP appearing in eq. (2). Integrating eq. (50) gives $\phi_{det}(t)$ which can then be inserted into eq. (52) so that

$$\phi_{det}(t) = \frac{at^2}{\hbar} + \omega_0 t \tag{53}$$

$$\phi_a(t) = \frac{at^2}{\hbar} + \omega_0 t + \frac{2}{n}Bt^n \quad . \tag{54}$$

We see that programming the generator that produces $\mathbf{E}_a(t)$ so that the phase $\phi_a(t)$ is given by eq. (54) causes a TRP sweep to be applied to the atom in the detector frame. Note that, to insure the two-level approximation is valid, the frequencies $\dot{\phi}_n(t)$ swept through by the TRP sweep should not include the resonance frequency of any other pair of atomic energy levels since this would drive unwanted dynamics not included in $\mathcal{H}(t)$.

Previous Work

Recently, Morton et. al. [23] showed how to use composite pulses to produce high fidelity single-qubit operations in electron paramagnetic resonance. The composite pulses are based on the BB1 corrective sequence [24]. Along with observation of non-decay of Rabi oscillations and suppression of secondary Fourier components in the spin echo decay envelope, they compared an improved Carr-Purcell pulse sequence (in which BB1 composite π-pulses replace ordinary π-pulses) with the Carr-Purcell-Meiboom-Gill sequence. From the decay of the echo produced by the improved Carr-Purcell sequence they inferred a fidelity for the BB1 π-pulses of $\mathcal{F} = 0.9999$. The authors noted that this fidelity is ultimately limited by pulse phase errors.

The fidelity in Ref. [23] is $\mathcal{F} = (1/2)\mathrm{Re}\left[Tr\left(U_a^\dagger U_t\right)\right]$. It is possible to relate our $Tr\,P$ upper bound on P_e to this fidelity. Recalling that $P = (U_a - U_t)^\dagger\,(U_a - U_t)$, we have

$$\begin{aligned} Tr\,P &= Tr\left(2 - \left[U_a^\dagger U_t + U_t^\dagger U_a\right]\right) \\ &= 4 - 2\,\mathrm{Re}\left[Tr\left(U_a^\dagger U_t\right)\right] \\ &= 4\,(1-\mathcal{F}) \quad , \end{aligned}$$

and so

$$\mathcal{F} = 1 - \frac{1}{4}\,Tr\,P \quad . \tag{55}$$

Using the results from Section 3 for $Tr\,P$ in eq. (55), we can determine the fidelity for the TRP gates:

$$\begin{aligned} \mathcal{F}_H &= 0.999998 \qquad (56)\\ \mathcal{F}_{V_P} &= 0.999980 \qquad (57)\\ \mathcal{F}_{V_{\pi/8}} &= 0.999992 \qquad (58)\\ \mathcal{F}_{NOT} &= 0.999997 \quad . \qquad (59) \end{aligned}$$

Future Work

(a) We are currently exploring whether TRP can be used to make a two-qubit gate that will complete the one-qubit gates considered here to give a set that: (i) is universal for quantum computation; and (ii) has all gates operating non-adiabatically with fidelities that yield $P_e < P_a$. A progress report on this work will be given elsewhere.

(b) Development of an approximate analytical approach to TRP would be very useful. We are not aware of any general tractable analytical approach to non-adiabatic rapid passage that could be used to find good starting simplexes for the sweep optimization procedure. It is because of this that we followed the numerical approach described above.

(c) Constructing a theory for the optimum twist profile $\phi(t)$ for a given quantum gate would also be a valuable contribution. To date, quartic twist has worked best, though we do not presently have arguments explaining why it will produce better gates than the other examples of TRP that we have considered, or whether some other profile will work even better.

(d) It would be especially interesting if the simulation results presented above could be tested experimentally. One possibility might be to use state tomography to measure the output density matrix $\rho_{exp} = U_a|\psi_0\rangle\langle\psi_0|\,U_a^\dagger$ resulting from an initial state $|\psi_0\rangle$, for each of the TRP generated gates U_a presented in Section 3. Associated with each sweep is a target gate U_t and a corresponding target density matrix $\rho_t = U_t|\psi_0\rangle\langle\psi_0|U_t^\dagger$. Having measured ρ_{exp}, evaluate the fidelity $\mathcal{F}(\rho_{exp}, \rho_t)$ [25]:

$$\mathcal{F}(\rho_{exp}, \rho_t) = Tr\sqrt{(\rho_{exp})^{1/2}\ \rho_t\ (\rho_{exp})^{1/2}}\quad . \tag{60}$$

Although this fidelity differs from the one considered in Ref. [23], one might naively anticipate that they are of comparable size. If so, then the experimentally determined fidelities should be close to the fidelities given in eqs. (56)–(59).

(e) The simulation results presented in this paper are for an isolated qubit interacting with a noiseless TRP sweep. Although this scenario might appear idealized, it seemed sensible to see what kind of performance was possible using TRP under the best possible conditions. One important extension would be to allow the TRP sweeps to include a noise component. To the extent that this noise leads to dephasing, TRP gate performance is expected to deteriorate once the dephasing time is of order the TRP inversion time T_0. Under these conditions, the qubit dynamics begins to loose its temporal phase coherence, and the quantum interference between alternatives begins to disappear. It would be worthwhile to consider simple noise models to study the sensitivity of TRP gate performance to parameters such as noise power and noise correlation time. A study along these lines was done for the quantum adiabatic search algorithm in Ref. [26]. Phase decoherence resulting from interaction of the target qubit with environmental qubits is another source of concern. As with the case of noise above, should the decoherence time be of order T_0, TRP gate performance is expected to suffer. Follow-up work that sheds light on how this performance cross-over occurs would be valuable.

Acknowledgments

M. Hoover was supported by the Illinois Louis Stokes Alliance for Minority Participation Bridge to the Doctorate Fellowship, and F. Gaitan thanks T. Howell III for continued support.

References

1. D. Gottesman, *Stabilizer codes and quantum error correction*, Ph. D. thesis, California Institute of Technology, Pasadena, CA (1997).
2. J. Preskill, *Reliable quantum computers*, Proc. R. Soc. Lond. A **454**, 385 (1998).
3. E. Knill, R. Laflamme, and W. H. Zurek, *Resilient quantum computation*, Science **279**, 342 (1998).

4. E. Knill, R. Laflamme, and W. H. Zurek, *Resilient quantum computation: error models and thresholds*, Proc. R. Soc. Lond. A **454**, 365 (1998).
5. D. Aharonov and M. Ben-Or, *Fault-tolerant computation with constant error*, in Proceedings of the Twenty-Ninth ACM Symposium on the Theory of Computing, 176 (1997).
6. A. Y. Kitaev, *Quantum computation algorithms and error correction*, Russ. Math. Surv. **52**, 1191 (1997).
7. A. Y. Kitaev, *Quantum error correction with imperfect gates*, in Quantum Communication, Computing, and Measurement (Plenum Press, New York, 1997), pp. 181-188.
8. D. Deutsch, *Quantum theory, the Church-Turing principle, and the universal quantum computer*, Proc. R. Soc. Lond. A **400**, 97 (1985).
9. D. Deutsch, *Quantum computational networks*, Proc. R. Soc. Lond. A **425**, 73 (1989).
10. A. Barenco et. al., *Elementary gates for quantum computation*, Phys. Rev. A **52**, 3457 (1995).
11. D. Deutsch, A. Barenco, and A. Ekert, *Universality in quantum computation*, Proc. R. Soc. Lond. A **449**, 669 (1995).
12. S. Lloyd, *Almost any quantum gate is universal*, Phys. Rev. Lett. **75**, 346 (1995).
13. P. O. Boykin et. al., *On universal and fault-tolerant quantum computing*, in Proc. 40th Ann. Symp. on Found. Comp. Sc., 486 (1999).
14. J. W. Zwanziger, S. P. Rucker, and G. C. Chingas, *Measuring the geometric component of the transition probability in a two-level system*, Phys. Rev. A **43**, 3232 (1991).
15. F. Gaitan, *Temporal interferometry: A mechanism for controlling qubit transitions during twisted rapid passage with possible application to quantum computing*, Phys. Rev. A **68**, 052314 (2003).
16. D. Suter et. al. , *Berry's phase in magnetic resonance*, Mol. Phys. **61**, 1327 (1987).
17. J. W. Zwanziger, U. Werner-Zwanziger, and F. Gaitan, *Non-adiabatic rapid passage*, Chem. Phys. Lett. **375**, 429 (2003).
18. F. Gaitan, *Berry's phase in the presence of a non-adiabatic environment with an application to magnetic resonance*, J. Mag. Reson. **139**, 152 (1999), see eq. [14].
19. R. P. Feynman and A. R. Hibbs, *Quantum Mechanics and Path Integrals* (McGraw-Hill, New York, 1965).
20. A. Shapere and F. Wilczek, *Geometric Phases in Physics* (World Scientific, New Jersey, 1989).
21. W. H. Press et. al. , *Numerical Recipes, 2nd. ed.* (Cambridge University Press, New York, 1992).
22. L. Allen and J. H. Eberly, *Optical Resonance and Two-Level Atoms* (Dover Publications, Inc. New York, 1987).
23. J. J. L. Morton et. al., *High fidelity single qubit operations using pulsed electron paramagnetic resonance*, Phys. Rev. Lett. **95**, 200501 (2005).
24. S. Wimperis, *Broadband, narrowband, and passband composite pulses for use in advanced NMR experiments*, J. Magn. Reson. Ser. A **109**, 221 (1994).
25. M. A. Nielsen and I. L. Chuang (2000), *Quantum Computation and Quantum Information*, Cambridge University Press (New York).
26. F. Gaitan, *Simulation of quantum adiabatic search in the presence of noise*, Int. J. Quantum Info. **4**, 843 (2006).